Article

A 3D CdTe QDs-DNA Nano-Reticulation as Highly Efficient Electrochemiluminescent Emitter for ultrasensitive Detection of MicroRNA from Cancer Cells

Manfei Sun, Jiali Liu, Yaqin Chai, Jin Zhang, Ying Tang, and Ruo Yuan

Anal. Chem., **Just Accepted Manuscript** • DOI: 10.1021/acs.analchem.9b01185 • Publication Date (Web): 28 May 2019

A 3D CdTe QDs-DNA Nano-Reticulation as Highly Efficient Electrochemiluminescent Emitter for ultrasensitive Detection of MicroRNA from Cancer Cells

Man-Fei Sun[†], Jia-Li Liu[†], Ya-Qin Chai[†], Jin Zhang[‡], Ying Tang[*,‡], Ruo Yuan[*,†]

[†]*Key Laboratory of Luminescent and Real-Time Analytical Chemistry (Southwest University), Ministry of Education, College of Chemistry and Chemical Engineering, Southwest University, Chongqing 400715, China.*

[‡]*Chongqing Key Laboratory of Environmental Materials and Remediation Technologies (Chongqing University of Arts and Sciences), Chongqing University of Arts and Sciences, Chongqing 402160, P.R. China.*

[*] Corresponding authors at: Tel.: +86 23 49891969, Fax: +86 23 61162725. Tel.: +86 23 68252277, Fax: +86 23 68253172.

E-mail addresses: tangying@cqwu.edu.cn (Y. Tang), yuanruo@swu.edu.cn (R. Yuan).

ABSTRACT

In this work, a novel three-dimensional CdTe QDs-DNA nano-reticulation (3D CdTe QDs-DNA-NR) was used as signal probe with the dual-legged DNA walker circular amplification as target conversion strategy to establish a pioneering electrochemiluminescence (ECL) biosensing strategy for ultrasensitive detection of microRNA-21 form cancer cells. Herein, such a 3D luminous nanomaterial with reticular structure, not only supported abundant CdTe QDs to avoid the inner filter effect for obtain a high ECL efficiency, but also contained the hemin/G-quadruplex as coreaction accelerator in the 3D CdTe QDs-DNA-NR/$S_2O_8^{2-}$ system for the enhancement of ECL intensity. Furthermore, with the target-induced dual-legged DNA walker circular amplification strategy, a mass of output DNA was produced to connect with the 3D CdTe QDs-DNA-NR for the construction of ECL biosensor, which realized the ultrasensitive detection of microRNA-21 from 100 aM to 100 pM and the detection limit down to 34 aM. Significantly, this work could be readily extended for the detection of other biomolecules to provide a neoteric channel for disease diagnosis.

INTRODUCTION

Electrochemiluminescence (ECL), presently, was widely reported in clinical laboratory diagnosis,[1,2] food safety supervision,[3] environmental pollution monitoring,[4] cell imaging,[5] and biosensing field[6] due to the high sensitivity, facile controllability, and simplified optical equipment.[7,8] To further boost the sensitivity of ECL sensor, nanomaterials[9,10] as signal amplification strategy played an increasingly important role for their excellent functions, for instance luminophore load,[11] biomolecules immobilization,[12] interface modification,[13] and enzyme simulation,[14] which have been extensively applied to construct ECL biosensors. Since Bard's group reported the first ECL study on quantum dots (QDs),[15] miscellaneous nanomaterials were extensively applied as ECL emitters.[16-18] Although these nanomaterials have the advantages of excellent immobilization capacity, the dense nanomaterials caused serious inner filter effect to reduce the ECL efficiency. Recently, we developed a self-enhanced ECL emitter by synthesizing a kind of hollow multihole polymeric nanospheres, which decreased inner filter effect of the bulk nanomaterials and achieved the enhancement on ECL efficiency.[19] However, the materials preparation was uncontrollable due to the successive wrapping of polyelectrolyte on SiO_2 nanoparticles. More importantly, the low space utilization of the hollow structure caused the decrease of loading capacity to limit the improvement of ECL signal. Hence, it is particularly significant to enhance the signal probe immobilization capacity on substrate and avoid the inner filter effect. Recently, the insertion[20] and label[21] of luminophore on the DNA nanomaterials[22-24] have been widely investigated, due to their favorable

biocompatibility, excellent controllability and easy editability. Nevertheless, the preparation of those luminous materials suffered from the complicated design of DNA, unstable embedding of luminophore and finite quantity of luminous probes, leading to the unstable and low ECL signal. Herein, the novel three-dimensional CdTe QDs-DNA nano-reticulation (3D CdTe QDs-DNA-NR) as highly efficient ECL emitter was assembled through the hemin/G-quadruplex to improve the stability and controllability of reticular nanomaterials, which not only increased the loading capacity of the CdTe QDs, but avoided the inner filter effect to significantly enhance the ECL efficiency. Furthermore, the hemin/G-quadruplex in the designed 3D CdTe QDs-DNA-NR was served as the coreaction accelerator[25,26] to notably enhance the ECL signal of the CdTe QDs-DNA-NR/$S_2O_8^{2-}$ system.[27]

Recently, DNA walkers has been increasingly received interests because such DNA nanomachine could efficiently self-assemble, autonomously walk, which hold a wide promise of practical application in nanomedicine, biosening, diagnostic systems.[28,29] For instance, Yang et al.[30] assembled a preeminent 3D DNA nanomachine through DNA modified Au nanoparticles (DNA-Au NPs), which made the single DNA walker move along the 3D DNA-AuNPs track to release payloads. Then, Zhang's group further developed a promising DNA walker nanomachine with thrombin binding to achieve quick and efficient detection of biomarkers.[31] However, those mentioned methods still existed a lot of defections, for instance, the restriction of single-legged DNA walker on free movement, the lower amplification efficiency, and the limitation of enzyme stability. To overcome the track limitations of

one-legged or leg-bound DNA walker, we proposed the target-induced dual-legged DNA walker circular amplification strategy to strongly improve the walk speed and amplification efficiency for producing a mass of output DNA, which provided an efficient target conversion tactic for ultrasensitive detection of microRNA-21 (miRNA-21).

Herein, combining the 3D CdTe QDs-DNA-NR as highly efficient ECL emitter and dual-legged DNA walker circular amplification as target conversion strategy, a novel ECL biosensor was constructed to detect miRNA-21 from cancer cells. Initially, the CdTe QDs were modified by DNA1 and CP DNA to form the CdTe QDs-DNA 1, while another CdTe QDs were connected with the DNA2 for obtaining CdTe QDs-DNA 2 (Scheme 1A). After the DNA hybridization process among the CdTe QDs-DNA 1, CdTe QDs-DNA 2, and linker DNA, the novel 3D CdTe QDs-DNA-NR was assembled and showed an excellent capacity of CdTe QDs and hemin/G-quadruplex for intense ECL emission in the CdTe QDs/$S_2O_8^{2-}$/hemin/G-quadruplex system (Scheme 1B). As shown in Scheme 1C, the AuNPs were electrodeposited on the sensing interface to immobilize DNA3 via Au-S bonds. Then, the 3D CdTe QDs-DNA-NR was introduced on the sensing surface of electrode based on the connection of CP DNA and DNA3 with the aid of output DNA originated from the target-induced dual-legged DNA walker circular amplification strategy (Scheme 1D-E). As depicted in Scheme 1E, when the target miRNA-21 unfolded hairpin 1 (H1) to bare the toehold, the toehold of H1 hybridized with hairpin 2 (H2) to form a dual-legged DNA walker with the release of miRNA-21 to unpack

another H1. Ulteriorly, the hybrid complexes (HC) of substrate DNA (ST) and assistant DNA (AS) were immobilized on the Au@Fe_3O_4 through the Au-S bond (HC-Au@Fe_3O_4) to support the tracks for dual-legged DNA walkers. Then, the dual-legged DNA walker could successfully hybridized with the ST to squeeze out the AS. Subsequently, with the participation of Nt. AIwI, the dual-legged DNA walker free walked on the HC-Au@Fe_3O_4 to operate the target-induced circular amplification strategy for the generation of numerous output DNA (Scheme 1D). Impressively, combining the excellent 3D CdTe QDs-DNA-NR as ECL emmiter and target-induced dual-legged DNA walker as amplification tactics, the ECL biosensor demonstrated a desirable assay to detect the target miRNA-21 ranging from 100 aM to 100 pM with a low limit of detection (34 aM). In general, the proposed biosensor affords the versatile sensing tactic for diverse biomolecules, which is hopefully applied in the disease diagnosis and clinical analysis.

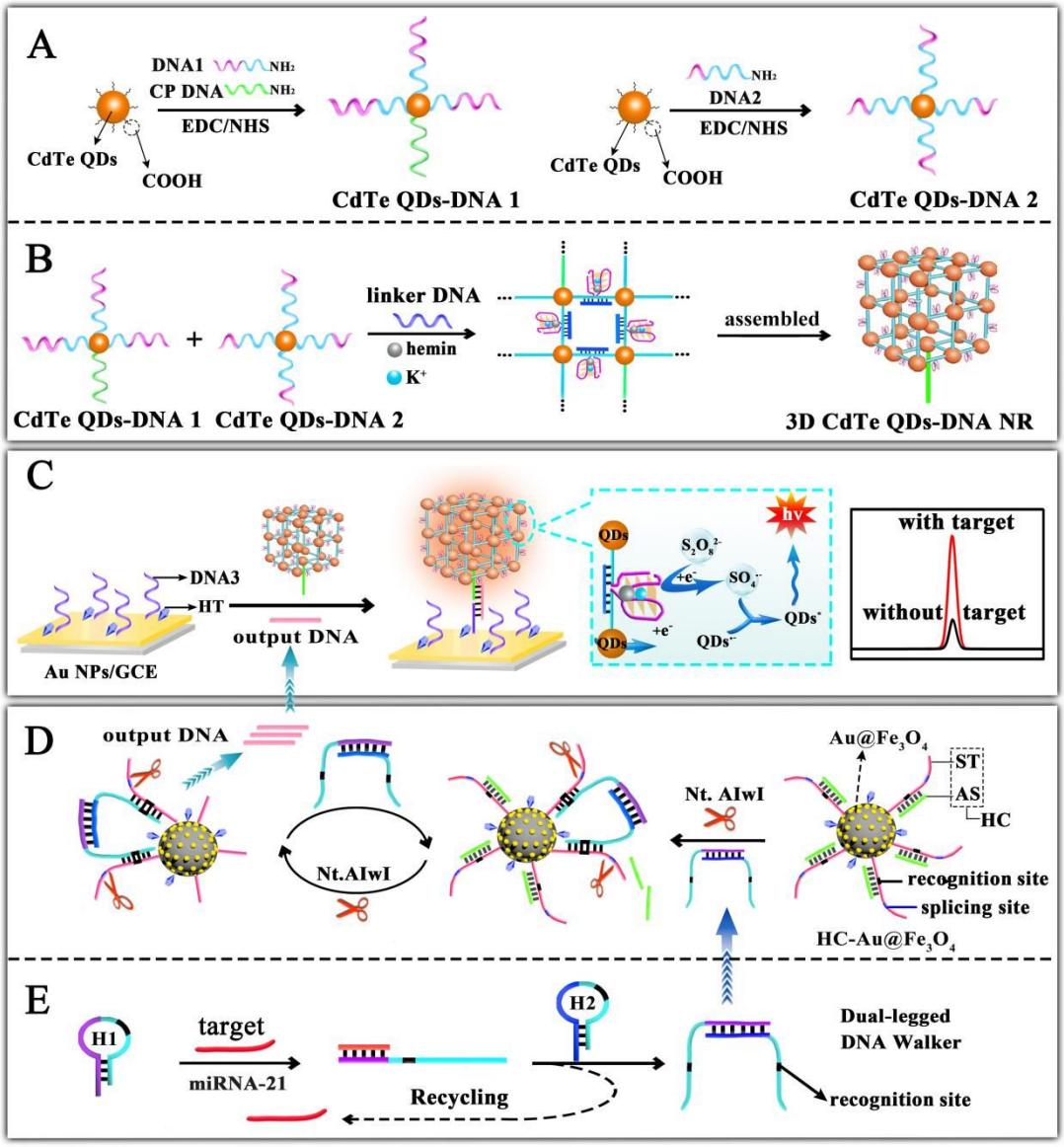

Scheme 1. Schematic Illustration of the Biosensor: (A-B) Preparation of 3D CdTe QDs-DNA-NR. (C) The Operating Principle of Biosensor for MicoRNA-21 Detection and Reaction Mechanism of ECL Biosensor. (D-E) Synthesis and Working Principle of Target-Induced Dual-legged DNA Walker Circular Amplification.

EXPERIMENTAL SECTION

Preparation of three-dimensional CdTe QDs-DNA nano-reticulation (3D QDs-DNA-NR). The CdTe quantun dots (QDs) were prepared according to classical method reported previously.[32] Typically, the CdTe QDs were dissolved in the 400 μL of HEPES buffer solution containing EDC (40 mM) with agitation at 4 °C for 20 min to activate the carboxyl group. Subsequently, the CdTe QDs-DNA 1 was prepared as follows: 20 μL of DNA1 (100 μM), 5 μL of capture DNA (CP DNA, 100 μM), the ratio between DNA1 and CP DNA was 1:4, and 5 μL of NHS (400 mM) were mixed with 170 μL of CdTe QDs solution (HEPES, pH=7.4) to oscillate for 5 h at 4 °C. Then, the CdTe QDs-DNA 2 was prepared as follows: 20 μL of DNA2 (100 μM) and 5 μL of NHS (400 mM) were mixed with 175 μL QDs (HEPES, pH=7.4) to agitate at 4 °C for 5 h. Thirdly, the linker DNA was diluted to 10 μM with HEPES buffer solution. Finally, 10 μL of CdTe QDs-DNA 1, 10 μL of CdTe QDs-DNA 2 and 10 μL of linker DNA (10 μM) were added into 70 μL HEPES (pH 9.0) containing 100 mM KCl and 5 ~ 20 μM hemin to react at 4 °C for 1 h. When the reaction was completed, the pure 3D CdTe QDs-DNA-NR was obtained by dialyzing in the dialysis bag (3.5 kD) at 4 °C for 48 h.

Target-induced dual-legged DNA-walker cycle amplification. Firstly, hairpin 1 (H1) and hairpin 2 (H2) were annealed at 95 °C to form hairpins, respectively. The mixture solution including assistant DNA (AS, 4 μM), and substrate DNA (ST, 2 μM) were annealed at 95 °C for 5 min and slowly cooled down to room temperature to

obtain hybrid complexes (HC). Then, 45 μL of HC, 10 μL of TCEP (10 mM) and 45 μL of Au@Fe_3O_4 were mixed to oscillate for 10 h at 4 °C. Afterwards, the HC-Au@Fe_3O_4 was obtained by magnetic separation to remove the supernatant. Subsequently, 40 μL of H1 (2 μM), 40 μL of H2 (2 μM), 1 μL of Nt. AIwI (10,000 U/mL), 9 μL of cutsmart buffer, and 10 μL of target microRNA-21 (miRNA-21) with different concentration were added to the HC-Au@Fe_3O_4 to incubate at 37 °C for 2 h, and sample solution (containing output DNA) was gained after magnetic separation, which was stored at 4 °C.

Preparation of the ECL Biosensor. Primally, the bare glassy carbon electrode (GCE) surface was scoured by the alumina powder (0.3 μm and 0.05 μm), and sequentially sonicated with deionized water and ethanol for 5 min to acquire a mirror-like GCE interface. After drying out, the bare GCE was electrodeposited for 30 s in 1% $HAuCl_4$ solution (-0.2 V) to obtain Au nanoparticles (Au NPs). Subsequently, 10 μL of DNA3 with sulfydryl group (SH, 2 μM) was connected with the Au NPs modified GCE at 4 °C for 12 h through Au-S bond. When the modified GCE was swashed with PBS buffer solution, 10 μL of HT (1 mM) was dropped on the above modified GCE and reacted for 40 min at room temperature to hinder the nonspecific sites. Ultimately, the prepared GCE was swashed with PBS buffer and stored at 4 °C.

Measurement Procedure. To measure the ECL signal, 10 μL of sample solution as well as 10 μL of the 3D CdTe QDs-DNA-NR solution were dropped onto the modified GCE and reacted at 37 °C for 2 h. Next, the biosensor was swashed with

PBS buffer solution and tested by the MPI-E multifunctional electrochemical analyzer in 50 mM $S_2O_8^{2-}$ solution with a sequential potential scanning from 0 V to -1.6 V at a scan rate of 100 mV s^{-1} and the voltage of the photomultiplier tube (PMT) at 800 V.

RESULTS AND DISCUSSION

The characteristic of the three-dimensional CdTe QDs-DNA nano-reticulation (3D CdTe QDs-DNA-NR). The morphology of the 3D CdTe QDs-DNA-NR was characterized. From the Figure 1A and Figure 1C, the TEM and SEM result indicated that the 3D CdTe QDs-DNA-NR with average diameters of 250 ± 30 nm and possessed a reticular nanostructure. Meanwhile, the 3D CdTe QDs-DNA-NR showed the uniform size in a larger field of view (Figure 1A,Figure 1A, Figure 1D). Obviously, compared to the particle size of single CdTe QDs (Figure S1), the 3D CdTe QDs-DNA-NR contained a large number of CdTe QDs, as shown in the images of Figure 1B and inset image of Figure 1A. Moreover, the HRTEM images inserted in Figure 1B exhibited a clear lattice fringe of 0.354 nm, which is in accordance with the lattice of the single CdTe QDs (insert image of Figure S1). As depicted in Figure 1D, the height of 3D CdTe QDs-DNA-NR is about 34.3 nm, which illustrated the single CdTe QDs are assembled into 3D reticular structure.

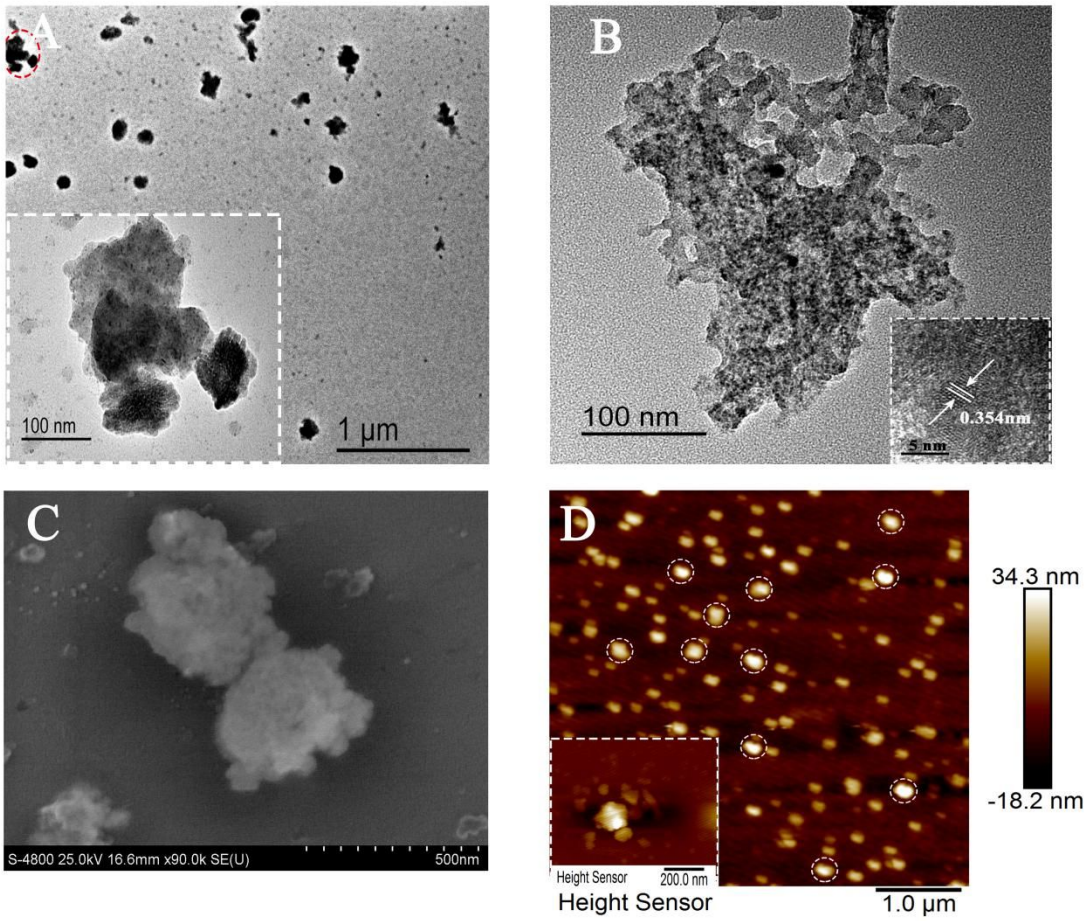

Figure 1. The TEM graphs of 3D CdTe QDs-DNA-NR (A). The HRTEM graph of 3D CdTe QDs-DNA-NR (B), the inset graph of (B): the lattice of CdTe QDs. The SEM graph of 3D CdTe QDs-DNA-NR (C). The AFM graphs of 3D CdTe QDs-DNA-NR (D).

Optical properties of CdTe QDs and 3D CdTe QDs-DNA-NR. The UV-vis spectrometer, fluorescence spectrophotometer and MPI-E ECL analyzer were employed to further explore the optical properties of the CdTe QDs and the 3D CdTe QDs-DNA-NR. The Figure 2A displayed the UV-vis absorption spectra of the CdTe QDs (Figure 2A, curve a) and 3D CdTe QDs-DNA-NR (Figure 2A, curve b). As demonstrated in the curve a, an obvious absorption peak appeared at 568 nm, indicating the characteristic absorption peak of CdTe QDs.[33] However, the specific

absorption peak of 3D CdTe QDs-DNA-NR became broader compared with that of CdTe QDs. Besides, an obvious absorption peak appeared at 260 nm, attributing to the characteristic absorption peak of DNA, which suggested the successful synthesis of 3D CdTe QDs-DNA-NR. As showed in the illustration of Figure 2A, the as-prepared CdTe QDs solution was light brown under ambient daylight, but exhibited red color with the 365 nm UV lamp radiation.

The fluorescence (FL) spectra of 3D CdTe QDs-DNA-NR was acquired by fluorescence spectrophotometer. As shown in Figure 2B, the maximum peak of FL emission was 630 nm. Furthermore, the ECL emission of 3D CdTe QDs-DNA-NR (Figure 2B-D) showed the ECL emission maximum wavelength at 700 nm via spectral analysis, which was consistent with previous reports.[34] Distinctly, the ECL maximum wavelength showed a red shift by 70 nm compared to the FL spectrum, which was caused by a major contribution of the surface states in ECL emission and instrumental differences.[35]

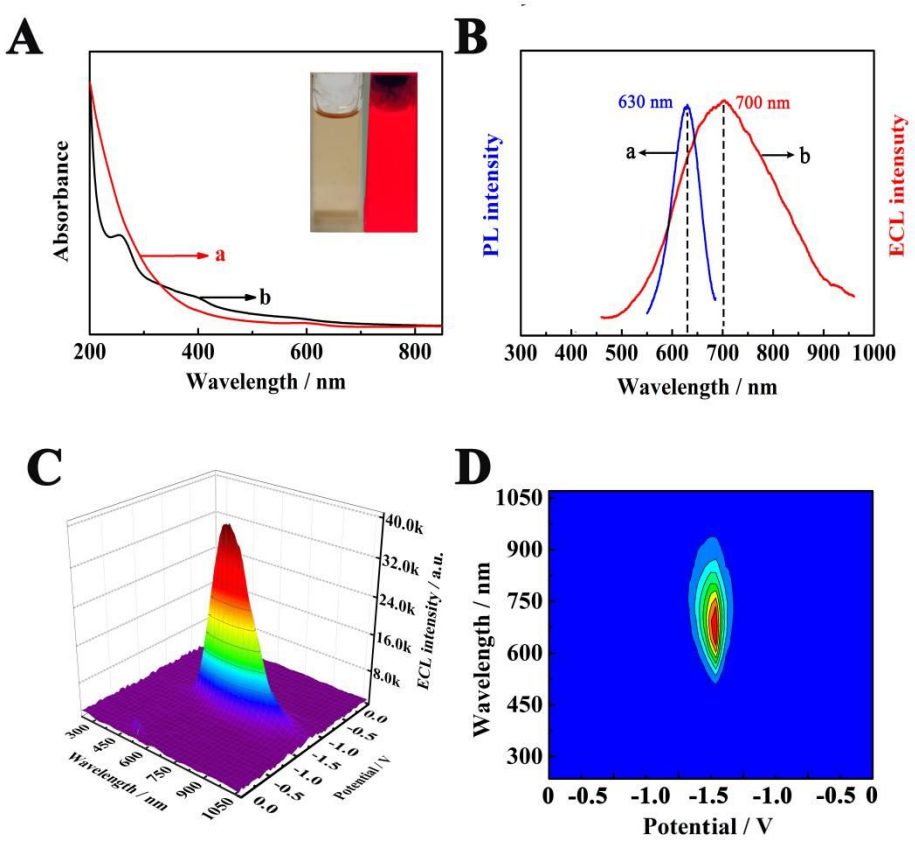

Figure 2. (A) The UV-vis absorption spectra of CdTe QDs (a) and 3D CdTe QDs-DNA-NR (b). The pictures of the CdTe QDs aqueous solution under visible light and 365 nm UV light (the illustration in Figure 2A). (B) The Fluorescence spectrum of 3D CdTe QDs-DNA-NR (a) emission spectrum (E_x = 350 nm) and ECL emission spectrum of 3D CdTe QDs-DNA-NR (b). The ECL-potential-wavelength results of the 3D CdTe QDs-DNA-NR in $S_2O_8^{2-}$ (50 mM) through the 3D surface image (C) and planar heat map (D).

Possible mechanism of the CdTe QDs/$S_2O_8^{2-}$/hemin/G-quadruplex system. Primarily, the ECL signals of different signal probes were characterized to prove the possible mechanism of this ECL system. As illustrated in Figure 3 (A-C), when the CdTe QDs signal probe was incubated on the GCE (curve a), a ECL signal of about 5019 a.u. was obtained. Remarkably, when the 3D CdTe QDs-DNA-NR (without

hemin) was incubated on the GCE, the ECL signal increased from 5109 a.u. to 9018 a.u. (Figure 3B), which indicated that plentiful CdTe QDs were encompassed in the 3D CdTe QDs-DNA-NR to provide a strong ECL signal. Most interestingly, after the hemin was introduced into the 3D CdTe QDs-DNA-NR to develop hemin/G-quadruplex structure, the ECL intensity of the 3D CdTe QDs-DNA-NR/$S_2O_8^{2-}$/hemin/G-quadruplex system was heightened significantly from 9018 a.u. to 15792 a.u. (Figure 3C, curve c), which indicated that the hemin/G-quadruplex as coreaction accelerator greatly enhanced the ECL emission in the 3D CdTe QDs-DNA-NR/$S_2O_8^{2-}$ system. Hence, the intense ECL signal of 3D CdTe QDs-DNA-NR attributed to the large quantities of CdTe QDs as luminophore and the hemin/G-quadruplex as a co-reaction accelerator in the 3D CdTe QDs-DNA-NR.

As depicted in the Figure 3D, the CV responses of the three different signal probes were employed to further prove the above ECL mechanism. Firstly, it could be seen in the that there was two redox peaks of the CdTe QDs signal probe (curve a). A reduction current was obvious increased at -0.82 V (curve b), which suggested that, compared with the CdTe QDs signal probe, the signal probe of the 3D CdTe QDs-DNA-NR (without hemin) to support abundant CdTe QDs for promoting electron transport. When the hemin (Fe^{III}) was interposed in the 3D CdTe QDs-DNA-NR, the reduction potential positively shifted from -0.82 V to -0.75 V (curve c) and the reduction current also increased, further proving that hemin made the reduction of $S_2O_8^{2-}$ easier and thereby resulted in the enhancement of $SO^{4-\bullet}$.

As shown in the Figure 3E, the possible ECL mechanism of the ECL binary system with CdTe QDs as luminophore and $S_2O_8^{2-}$as coreactant was proposed as follows: Firstly, the electroreduction of $S_2O_8^{2-}$ and CdTe QDs produced a spot of $SO_4^{\bullet-}$ and CdTe QDs$^{\bullet-}$, respectively. Then, the $SO_4^{\bullet-}$ reacted with the CdTe QDs$^{\bullet-}$ to generate an excited-state CdTe QDs* for the ECL emission. Subsequently, when the hemin (Fe^{III}) was interposed in the 3D CdTe QDs-DNA-NR, a ternary ECL system was consisted with the CdTe QDs, $S_2O_8^{2-}$ and hemin/G-quadruplex. Herein, the hemin (Fe^{III}) in the G-quadruplex as coreaction accelerator interacted with the $S_2O_8^{2-}$ to generate more $SO_4^{\bullet-}$ and hemin (Fe^{II}). Finally, plenty of $SO_4^{\bullet-}$ reacted with CdTe QDs$^{\bullet-}$ (produced by electrical reduction of CdTe QDs) to generate abundant CdTe QDs* for intense ECL emission. Thus, the possible ECL mechanisms of the 3D CdTe QDs-DNA-NR/$S_2O_8^{2-}$/hemin/G-quadruplex system were shown in Figure 3F.

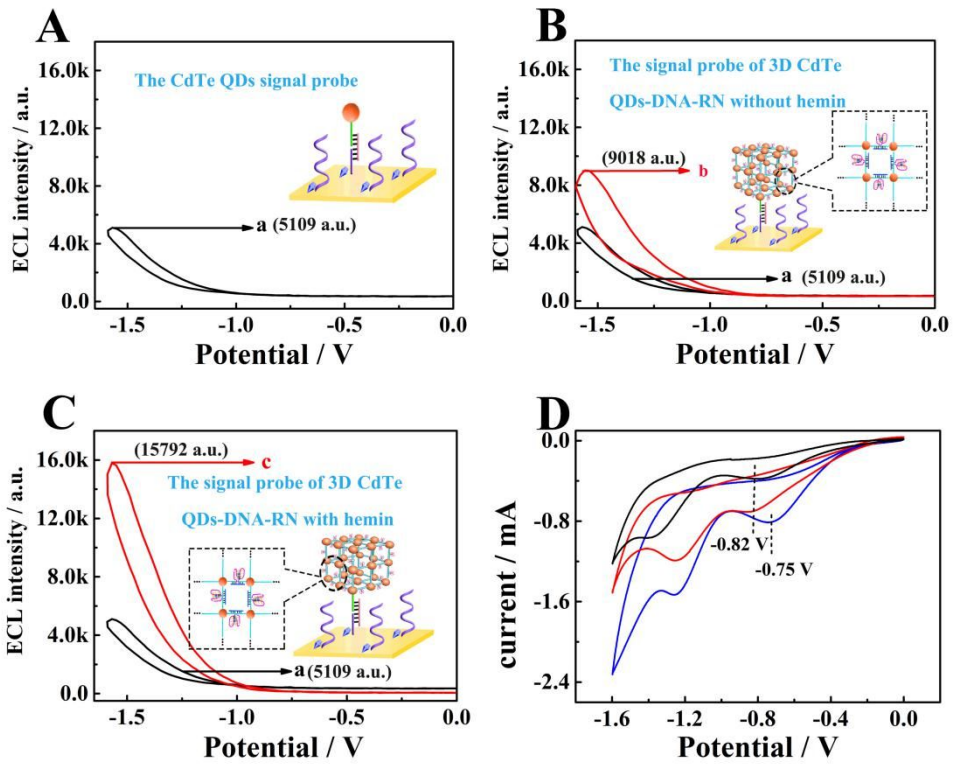

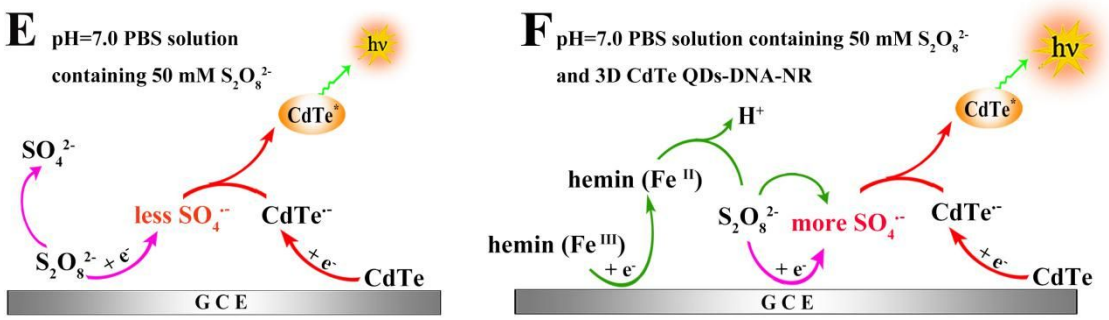

Figure 3. The ECL curves (A-C) and the CV responses (D) of the CdTe QDs signal probe (curve a), the 3D CdTe QDs-DNA-NR without hemin (curve b), and the 3D CdTe QDs-DNA-NR with hemin (curve c).The possible ECL mechanism of the CdTe QDs/$S_2O_8^{2-}$ system (E) and the 3D CdTe QDs-DNA-NR/$S_2O_8^{2-}$ system (F).

Optimization of the ECL biosensor. The amount of hemin, the incubation time, the incubation time of Nt. AIwI, and the ratio between DNA1 and CP DNA of ECL biosensor have great effects on the ECL luminous efficiency. Therefore, the four vital experimental conditions were researched to obtain the optimal experimental. The optimization condition study of the incubation time of Nt. AIwI, and the ratio between DNA1 and CP DNA was presented in the supporting information (SI). The ECL signal changed gradually as the concentration of hemin increases as depicted in the Figure 4A. When the concentration of hemin reached at 10 μM, the maximum ECL signal was observed because hemin had the catalytic effect on the basic of the redox of Fe^{III}/Fe^{II}.[36] However, when the hemin concentration exceeds 10 μM, the ECL signal was gradually reduced, since the hemin had the function of electron transfer quencher at higher concentration.[37,38] Hence, the optimal concentration of hemin was 10 μM and was applied to the next experiments. Meanwhile, as exhibited in the

Figure 4B, as the increase of incubation time among the DNA3, sample solution (containing the output DNA) and the 3D CdTe QDs-DNA-NR, the ECL intensity increased gradually, due to the combination of abundant 3D CdTe QDs-DNA-NR to the electrode. After the incubation time was over 2 h, the ECL signal was stable eventually. Therefore, the optimal incubation time is 2 h to apply in the whole experiments.

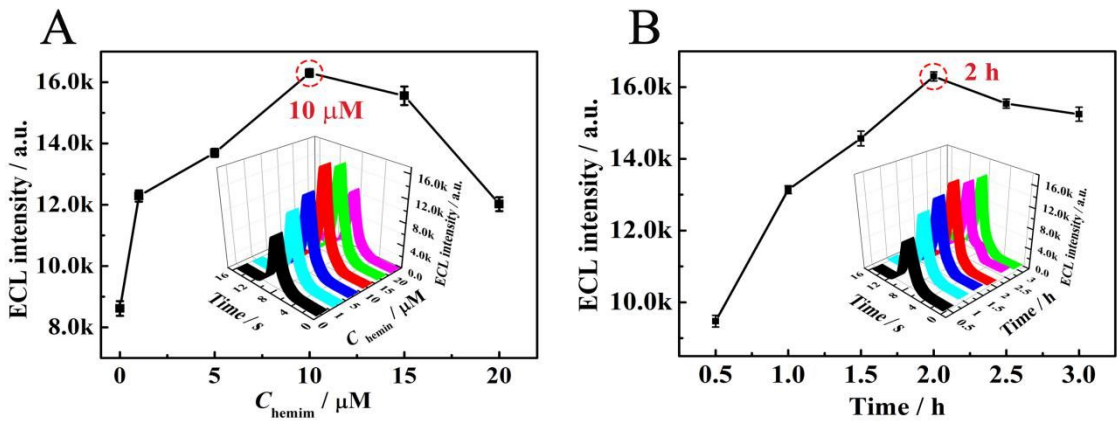

Figure 4. The optimization of (A) the concentration of hemin and (B) the incubation time of ECL biosensor fabrication at 100 pM miRNA-21. Error bars, SD, $n = 3$.

Detection of miRNA-21 with the Proposed Biosensor. Under optimal conditions, the quantitative experiment of designed ECL biosensor to different concentrations of microRNA-21 (miRNA-21) was detected on the basis of the "signal-on" schema. The calibration curve demonstrated a satisfactory linear relationship between the ECL intensity and the logarithm of miRNA-21 concentrations in the range of 100 aM to 100 pM (a correlation coefficient is 0.9989), as depicted in the Figure 5A. The linear regression equation is $I = 1781.08 \lg (c/\mathrm{M}) + 33507.61$, which showed a low detection limit of 34 aM. As shown in Table 1,

compared to the existing miRNAs detection methods, the designed biosensor provided a more effective way and a higher sensitivity to quantify miRNA-21.

Table 1. Comparison for the designed work and other microRNA detection methods.

Measurement technique	Target	Linear range	Detection limit	Reference
Electrochemical	microRNA-21	1.0 fM to 10 nM	0.31 fM	39
Fluorescence	microRNA-21	0 fM to 500 fM	3.0 fM	40
Raman	microRNA-21	10 fM to 100 pM	10 fM	41
ECL	microRNA-141	1 fM to 100 pM	1.0 fM	42
ECL	microRNA-21	10 fM to 0.1 nM	3.3 fM	21
ECL	microRNA-21	100 aM to 100 pM	34 aM	This work

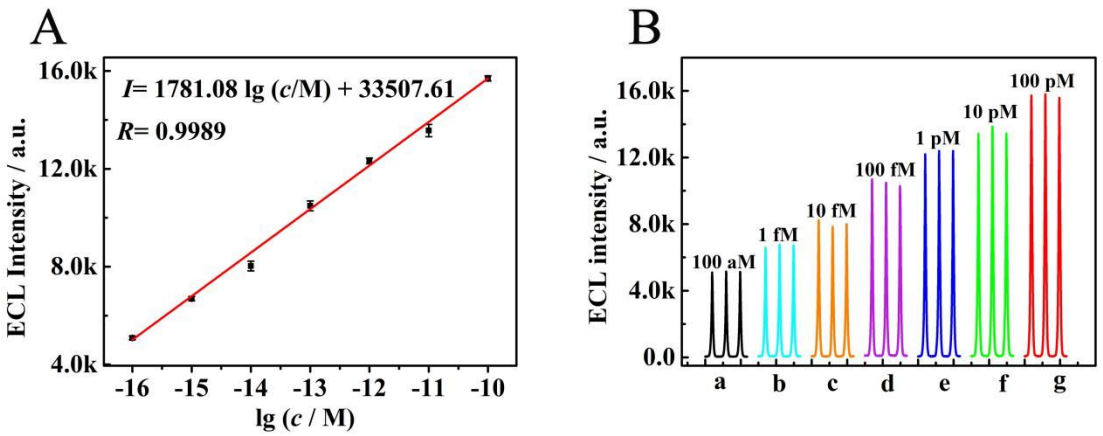

Figure 5. (A) The calibration plot of miRNA-21 detection (in the $S_2O_8^{2-}$ (50 mM) solution) Error bars, SD, *n*=3. (B) The ECL response curves of the designed biosensor at concentrations of miRNA-21 ranging from 100 aM to 100 pM, *n*=3.

Stability and selectivity of the ECL biosensor. The stability of the biosensor was tested at the optimalizing conditions. The continuous circulating voltage was used to scan the biosensor for 20 cycles at a speed of 100 $mV \cdot s^{-1}$. As depicted in the Figure 6A, after 20 cycles of cyclic scanning, the ECL signal has no significant change (1fM

of miRNA-21 concentration), indicating that the biosensor has good stability (R=0.605%). In addition, the influences of other miRNAs (microRNA-126 (miRNA-126), microRNA-155 (miRNA-155), and microRNA-141 (miRNA-141)) were explored to assess the selectivity of designed biosensor. Different reaction solutions containing miRNA-126 (10 pM), miRNA-155 (10 pM), miRNA-141 (10 pM), miRNA-21 (1 pM), and the mixture (containing miRNA-21 (1 pM), miRNA-126 (10 pM), miRNA-155 (10 pM) and miRNA-141 (10 pM)) were respectively incubated on the biosensor for 2 h at 37 ^{o}C. Compared with the blank (replaced the miRNA-21 with HEPES buffer solution, other operations were unchanged), the miRNA-126, miRNA-155 and miRNA-141 revealed a little effects on ECL response, as shown in the Figure 6B. The signal of mixture solution had no remarkable difference with that of the 1 pM miRNA-21, which demonstrated miRNA-126, miRNA-155 and miRNA-141 showed unconspicuous influence on the miRNA-21 detection. Those results showed that the designed biosensor had excellent stability and selectivity on the miRNA-21 detection.

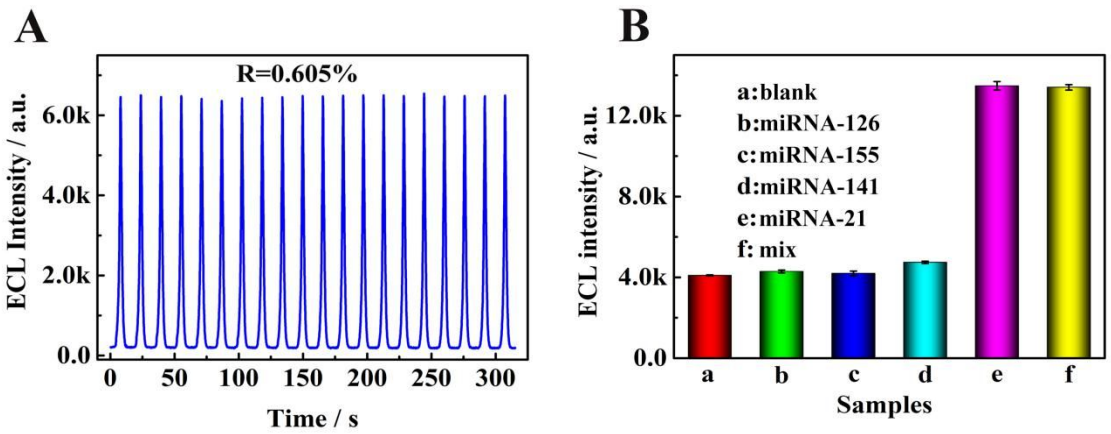

Figure 6. (A) The ECL signals-time curve of the proposed biosensor under a continuous scan with

20 cycles in the $S_2O_8^{2-}$ solution (50 mM). (B) Selectivity of the ECL biosensor with diverse miRNAs. Error bars, SD, *n*=3.

Application of the biosensor in cancer cells. The ECL test was carried out in the extracts of cervical cancer cells (Hela) and the human breast cancer cells line (MCF-7) to attest the capability of the proposed ECL biosensor. The cell sample extracts were obtained with the aid of commercial microRNA extraction kits. To investigate the ECL responses, the ECL signal with cell concentration ranging from 10^1 cells to 10^6 cells were studied (Figure 7). When the concentrations of Hela cells increased from 10^1 cells to 10^6 cells, a slight increase in the ECL response was observed, which illustrated that miRNA-21 exhibited low expression in Hela cells. Obvious ECL response changes were observed when the concentration of MCF-7 cells varied from 10^1 cells to 10^6 cells, suggesting the high expression of miRNA-21 in the MCF-7 cells. The results showed that the miRNA-21 was higher expressed in MCF-7 cells than Hela cells conforming to the reported work.[43] Hence, the proposed strategy could be applied in the detection of miRNA-21 from cancer cells.

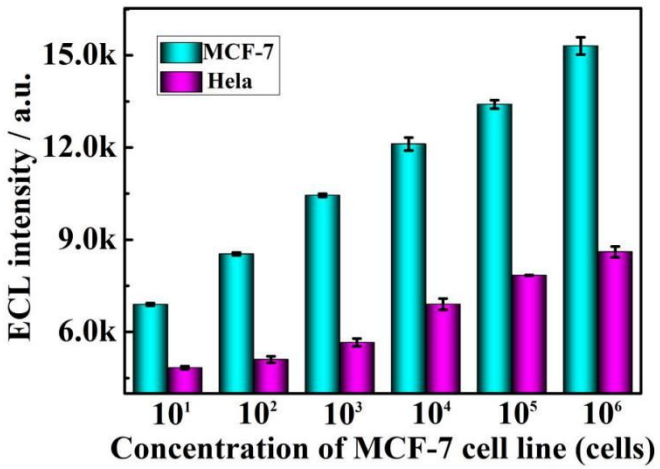

Figure 7: Application of the biosensor in the extracts of MCF-7 cell line and Hela cell line.

CONCLUSIONS

In this work, a ECL biosensing platform for the ultrasensitive detection of microRNA-21 (miRNA-21) has been demonstrated based on three-dimensional CdTe QDs-DNA nano-reticulation (3D CdTe QDs-DNA-NR) as ECL signal probe and highly efficient dual-legged DNA walker circular amplification as target conversion strategy. Significantly, the as-prepared 3D CdTe QDs-DNA-NR was linked through the hemin/G-quadruplex, which achieved notable improvement of ECL efficiency from two aspects. Firstly, the 3D CdTe QDs-DNA-NR not only effectively supported abundant QDs, but also greatly avoided the inner filter effect to realize an intensive ECL emission. Secondly, the hemin/G-quadruplex in the 3D CdTe QDs-DNA-NR improved the stability of the reticular nanostructure, and served as coreaction accelerator in the $S_2O_8^{2-}$ system for further improving the ECL efficiency. Meanwhile, with the target-induced dual-legged DNA walker cycle amplification, a large number of output DNA were outputted to assemble the 3D CdTe QDs-DNA-NR for constructing the ECL biosensor, which exhibited high sensitivity for the detection of miRNA-21. Furthermore, this protocol offered a preeminent sensing strategy for bioanalysis and had great application prospects in the biomedicine detection and clinical diagnosis.

ASSOCIATED CONTENT

Supporting Information

Reagents and materials, **a**pparatus, Cell culture and lysis, polyacrylamide gel electrophoresis (PAGE) analysis, the characteristic of the CdTe QDs, the characteristic of CdTe QDs-DNA 1 and CdTe QDs-DNA 2, optimization of the ratio between DNA1 and CP DNA, and the incubation time of Nt. AIwI, typical PAGE characterization of the target-induced dual-legged DNA-walker cycle amplification strategy, and electrochemical behaviors of ECL biosensor were supplied in Supporting Information.

AUTHOR INFORMATION

*** Corresponding authors**

*Tel.: +86 23 68252277, Fax: +86 23 68253172. E-mail: yuanruo@swu.edu.cn (R. Yuan).

*Tel.: +86 23 49891969, Fax: +86 23 61162725. E-mail: tangying@cqwu.edu.cn (Y. Tang).

Notes

The authors declare no competing financial interest.

Acknowledgements

This work was financially supported by the NNSF of China (21775124, 21575116, 21675129, 51473136), and the Fundamental Research Funds for the

Central Universities (XDJK2018AA0003), China, and the Chongqing Science and Technology Commission of China (cstc2015jcyjBX0126, cstc2016shmsZX20001).

REFERENCES

(1) Zhou, X. M.; Zhu, D. B.; Liao, Y. H.; Liu, W. P.; Liu, H. X.; Ma, Z. K.; Xing, D. *Nat. Protoc*. **2014**, 9, 1146-1159.

(2) Liu, S. S.; Yuan, H. X.; Bai, H. T.; Zhang, P. B.; Lv, F. T.; Liu, L. B.; Dai, Z. H.; Bao, J. C.; Wang, S. *J. Am. Chem. Soc*. **2018**, *140*, 2284-2291.

(3) Li, W. L.; Kong, F. Z.; Zhang, Q.; Liu, W. W.; Kong, H.; Liu, X. P.; Khan, M. I.; Wahid, A.; Saud, S.; Xiao, H.; Cao, C. X.; Fan, L. Y. *Anal. Chem*. **2018**, *90*, 6710-6717.

(4) Cai, F. D.; Zhu, Q.; Zhao, K.; Deng, A. P.; Li, J. G. *Environ. Sci. Technol*. **2015**, *49*, 5013-5020.

(5) Voci, S.; Goudeau, B.; Valenti, G.; Lesch, A.; Jović, M.; Rapino, S.; Paolucci, F.; Arbault, S.; Sojic, N. *J. Am. Chem. Soc*. **2018**, 140, 14753-14760.

(6) Chen, M. M.; Wang, Y.; Cheng, S. B.; Wen, W.; Zhang, X. H.; Wang, S. F.; Huang, W. H. *Anal. Chem*. **2018**, *90*, 5075-5081.

(7) Richter, M. M. *Chem. Rev*. **2004**, *104*, 3003-3036.

(8) Maar, R. R.; Zhang, R. Z.; Stephens, D. G.; Ding, Z. F.; Gilroy, J. B. *Angew. Chem.* **2018**, *130*, 1-6.

(9) Chang, Y. L.; Palacios, R. E.; Fan, F. R. F.; Bard, A. J.; Barbara, P. F. *J. Am. Chem. Soc*. **2008**, *130*, 8906-8907.

(10) Hesari, M.; Ding, Z. F. *Acc. Chem. Res*. **2017**, *50*, 218-230.

(11) Long, X. Y.; Zhang, F.; He, Y. P.; Hou, S. F.; Zhang, B.; Zou, G. Z. *Anal. Chem*. **2018**, *90*,

3563-3569.

(12) Hanan, A. K.; Silvia, V.; Liza, R.; Neso, S.; Klaus, M. *Chem. Sci*. **2018**, *9*, 8946-8950.

(13) Qiao, Y. L.; Li, Y.; Fu, W.; Guo, Z. H.; Zheng, X. W. *Anal. Chem*. **2018**, *90*, 9629-9636.

(14) Liu, J. L.; Tang, Z. L.; Zhuo, Y.; Chai, Y. Q.; Yuan, Ruo. *Anal. Chem*. **2017**, *89*, 9108-9115.

(15) Ding, Z. F.; Quinn, B. M.; Haram, S. K.; Pell, L.E.; Korgel, B. A.; Bard, A. J. *Science.* **2002**, *296*, 1293-1297.

(16) Zhu, X. Q.; Zhai, Q. F.; Gu, W. L.; Li, J.; Wang, E. K. *Anal. Chem*. **2017**, *89*, 12108-12114.

(17) Dong, Y. P.; Chen, G.; Zhou, Y.; Zhu, J. J.; *Anal. Chem*. **2016**, *88*, 1922-1929.

(18) Zhao, M.; Chen, A. Y.; Huang, D.; Zhuo, Y.; Chai, Y. Q.; Yuan, R. *Anal. Chem*. **2016**, *88*, 11527-11532.

(19) Chen, A. Y.; Zhao, M.; Zhuo, Y.; Chai, Y. Q.; Yuan, R. *Anal. Chem*. **2017**, *89*, 9232-9238.

(20) Wang, H. J.; Yuan, Y. L.; Zhuo, Y.; Chai, Y. Q.; Yuan, R. *Anal. Chem*. **2016**, *88*, 5797-5803.

(21) Zhang, P.; Jiang, J.; Yuan, R.; Zhuo, Y.; Chai, Y. Q.; *J. Am. Chem. Soc*. **2018**, *140*, 9361-9364.

(22) Li, S. K.; Chen, A. Y.; Niu, X. X.; Liu, Z. T.; Du, M.; Chai, Y. Q.; Yuan, R.; Zhuo, Y. *Chem. Commun*. **2017**, *53*, 9624-9627.

(23) Zhu, G. Z.; Hu, R.; Zhao, Z. L.; Chen, Z.; Zhang X. B.; Tan, W. H. *J. Am. Chem. Soc*. **2013**, *135*, 16438.

(24) Wu, F. F.; Zhou, Y.; Zhang, H.; Yuan, Ruo.; Chai, Y. Q. *Anal. Chem*. **2018**, *90*, 2263-2270.

(25) Ma, M. N.; Zhuo, Y.; Yuan, R.; Chai, Y. Q. *Anal. Chem*. **2015**, *87*, 11389-11397.

(26) Zhou, Y.; Chen, S. H.; Luo, X. L.; Chai, Y. Q.; Yuan, R. *Anal. Chem*. **2018**, *90*, 10024-10030.

(27) Zeng, W. J.; Liao, N.; Lei, Y. M.; Zhao, J.; Chai, Y. Q.; Yuan, Ruo.; Zhuo, Y. *Biosens. Bioelectron*. **2018**, *100*, 490-496.

(28) Zhou, C.; Duan, X. Y.; Liu, N. *Nat. Commun*. **2015**, *6*, 8102.

(39) Jung, C.; Allen, P. B.; Ellington, A. D. *Nature Nanotech*. **2016**, *11*, 157-163.

(30)Yang, X. L.; Tang, Y. N.; Mason, S. D.; Chen, J. B.; Li, F. *ACS Nano*. **2016**, *10*, 2324-2330.

(31) Ji, Y. H.; Zhang, L.; Zhu, L. Y.; Lei, J. P.; Wu, J.; Ju, H. X. *Biosens. Bioelectron*. **2017**, *96*, 201-205.

(32) Yang, X.; Yu, Y. Q.; Peng, L. Z.; Lei, Y. M.; Chai, Y. Q.; Yuan, R. *Anal. Chem*. **2018**, *90*, 3995-4002.

(33) Li, M. J.; Xiong, C.; Zheng, Y. N.; Liang, W. B.; Yuan, R.; Chai, Y. Q. *Anal. Chem*. **2018**, *90*, 8211-8216.

(34) Yu, Y. Q.; Zhang, H. Y.; Chai, Y. Q.; Yuan, R.; Zhuo, Y. *Biosens. Bioelectron*. **2016**, *85*, 8-15.

(35) Myung, N.; Bae, Y.; Bard, A. J. *Nano Lett*. **2003**, *3*, 1053-1055.

(36) Liu, Y. Q.; Xiong, E. H.; Li, X. Y.; Li, J. J.; Zhang, X. H.; Chen, J. H. *Biosens. Bioelectron*. **2017**, *87*, 970-975.

(37) Yuan, R.; Yu, X. L.; Zhang, Y.H.; Xu, L. L.; Cheng, W.; Tu, Z.G.; Ding, S. J. *Biosens. Bioelectron*. **2017**, *92*, 342-348.

(38) Zhao, M.; Liao, N.; Zhuo, Y.; Chai, Y. Q.; Wang, J. P.; Yuan, R. *Anal. Chem*. **2015**, *87*, 7602-7609.

(39) Zhang, X. L.; Yang, Z. H.; Chang, Y. Y.; Qing, M.; Yuan, R.; Chai, Y. Q. *Anal. Chem*. **2018**, *90*, 9538-9544.

(40) Xia, Y. K.; Wang, L. L; Li, J.; Chen, X. Q.; Lan, J. M.; Yan, A.; Lei, Y.; Yang, S.; Yang, H. H.; Chen, J. H. *Anal. Chem*. **2018**, *90*, 8969-8976.

(41) Su, J.; Wang, D. F.; Nörbel, L.; Shen, J. L.; Zhao, Z. H.; Dou, Y. Z.; Peng, T. H.; Shi, J.; Mathur, S.; Fan, C. H.; Song, S. P. *Anal. Chem*. **2017**, *89*, 2531-2538.

(42) Wang, Y. Z.; Ji, S. Y.; Xu, H. Y.; Zhao, W.; Xu, J. J.; Chen, H. Y. *Anal. Chem*. **2018**, *90*, 3570−3575.

(43) Ying, Z. M.; Wu, Z.; Tu, B.; Tan, W. H.; Jiang, J. H. *J. Am. Chem. Soc*. **2017**, *139*, 9779-9782.

For TOC only

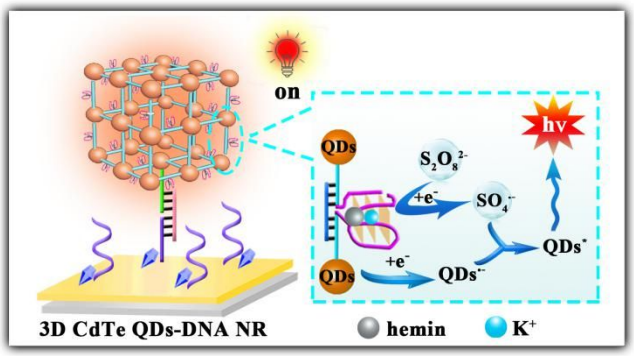
on
QDs
$S_2O_8^{2-}$
+e⁻
$SO_4^{\cdot-}$
hv
QDs*
+e⁻
QDs
QDs⁻
3D CdTe QDs-DNA NR
hemin
K^+